



Vapor-fumigation for record efficiency two-dimensional perovskite solar cells with superior stability

Journal:	<i>Energy & Environmental Science</i>
Manuscript ID	EE-COM-08-2018-002284.R1
Article Type:	Communication
Date Submitted by the Author:	29-Sep-2018
Complete List of Authors:	<p>Zhu, Xuejie; Shaanxi Normal University Xi'an, Shaanxi, CN Xu, Zhuo; Shaanxi Normal University, Key Laboratory of Applied Surface and Colloid Chemistry, Ministry of Education; Shaanxi Key Laboratory for Advanced Energy Devices; Shaanxi Engineering Lab for Advanced Energy Technology, School of Materials Science and Engineering Zuo, Shengnan; Shaanxi Normal University Feng, Jiangshan; Shaanxi Normal University Xi'an, Shaanxi, CN Wang, Ziyu; Dalian Institute of Chemical Physics zhang, rong; Shaanxi Normal University, Key Laboratory of Applied Surface and Colloid Chemistry, MOE, School of Materials Science and Engineering Zhao, Kui; Shaanxi Normal University, Key Laboratory of Applied Surface and Colloid Chemistry, MOE, School of Materials Science and Engineering Zhang, Jian; Guilin University of Electronic Technology, Liu, Hairui; Pennsylvania State University Priya, Shashank; Pennsylvania State University, Department of Materials Science and Engineering Liu, Shengzhong; Shaanxi Normal University, Key Laboratory of Applied Surface and Colloid Chemistry, MOE, School of Materials Science and Engineering; Dalian Institute of Chemical Physics, Chinese Academy of Sciences, Yang, Dong; Shaanxi Normal University, School of Materials Science and Engineering; Pennsylvania State University, Department of Materials Science and Engineering</p>

COMMUNICATION

Vapor-fumigation for record efficiency two-dimensional perovskite solar cells with superior stability

Cite this: DOI: 10.1039/x0xx00000x

Received 00th January 2012,
Accepted 00th January 2012

DOI: 10.1039/x0xx00000x

www.rsc.org/

Xuejie Zhu,^a Zhuo Xu,^a Shengnan Zuo,^a Jiangshan Feng,^a Ziyu Wang,^b Xiaorong Zhang,^a Kui Zhao,^a Jian Zhang,^d Hairui Liu,^c Shashank Priya,^{*c} Shengzhong (Frank) Liu^{*a,b} and Dong Yang^{*a,c}

Two-dimensional (2D) perovskites have emerged as prospective candidates for high performance perovskite solar cells (PSCs) due to their remarkable environmental stability. However, their power conversion efficiency (PCE) is much lower than their 3D counterparts owing to large exciton binding energy, poor carrier transport, and low conductivity. Herein, we developed methylammonium (MA) based 2D perovskite thin film using vapor-fumigation technology. Compared to traditional 2D perovskite based on bulky butylammonium (BA) cations, its exciton binding energy significantly decreased to 172 meV from 510 meV, as calculated by the first-order perturbation theory and an infinite barrier approximation, due to the high dielectric constant of MA. According to the WKb approximation, the tunneling probability of a carrier through a quantum wells increased by four orders of magnitude because of the smaller layer thickness, which was confirmed by XRD (the layer spacing decreased to 9.08 Å of MA₂PbI₄ from 13.39 Å of BA₂PbI₄). In addition, theoretical calculation and experimental analysis reveal that MA₂PbI₄ perovskite possesses a narrow band gap, good conductivity, and low trap density. As a result, the PCE of the 2D PSCs reached 16.92%, and certified efficiency was 16.6% by the National Institute of Metrology (NIM), the highest efficiency value so far for 2D PSCs. Furthermore, the MA₂PbI₄ devices exhibited superior long-term stability under illumination and exposure to environmental conditions. The PCEs of the 2D perovskite devices without encapsulation degraded by only 2.2% from their initial values when exposed to ambient conditions at ~55% relative humidity for 1512 hours. Meanwhile, the efficiency maintained 97.2% of its initial value when the device was continuously illuminated for 500 hours at 60 °C in Argon. Even after following the illumination test with light-soaking for over 500 h in ambient air, the PCE of the unsealed device suffered only a minor degradation of 3.8%.

Perovskite solar cells (PSCs) based on three-dimensional (3D) absorbers have been attracting considerable attention owing to their extremely high power conversion efficiency (PCE) and simple fabrication process.¹⁻¹¹ However, their environmental instability has been a major challenge for commercialization.^{12,13} Ruddlesden-Popper two-dimensional (2D) perovskite materials, with strong photo- and chemical-stability, large exciton binding energies and continuous tunability of their optoelectronic properties due to the beneficial geometric effect and dielectric contrast effect,¹⁴ have been successfully applied in photovoltaics and optoelectronics.¹⁵⁻¹⁷ To date, the 2D PSCs have shown a lower PCE of 15.3%,¹⁸ which is caused by the large exciton binding energy and quantum well (QW) in out-of-plane direction. Further efficiency improvement with excellent stability requires reduction of the exciton binding energy and QW effect in the 2D perovskites.

The 2D perovskite materials, with the general chemical formula (RNH₃)₂PbX₄, where R is an organic chain and X is a halogen, consist of lead halide layers inserted between organic barrier planes of RNH₃. In the 2D perovskite semiconductors, the van der Waals interaction between organic cations and inorganic anions is so large that it takes more energy to destroy the 2D crystal structure,¹⁹⁻²¹ leading to excellent stability compared to the 3D perovskites. Furthermore, 2D perovskite materials often employ more hydrophobic bulkier organic cations instead of the short alkyl chain organic cations typically used in the 3D perovskites, which can significantly improve their stability to moisture.²² Unfortunately, the thickness of the 2D network decreases to the scale of the de Broglie wavelength of the carriers, giving a quantum confinement effect on the charge behavior and creating a typical QW structure, which halves the Bohr radius and quadruples the exciton binding energy.²³ Furthermore, the great difference between the dielectric constants of the inorganic and organic layers greatly increases the exciton binding energy.²⁴ During photovoltaic operation, the geminate recombination loss would increase due to the large binding energy, which leads to reduced charge dissociation into free carriers. For example, the 2D perovskites based on (C₆H₅C₂H₄NH₃)₂PbI₄ in early efforts suffered from exciton binding energies as high as several hundred millielectron volt, too large for photovoltaic applications;²⁵⁻²⁷ even though they were assembled into solar cells, the efficiency

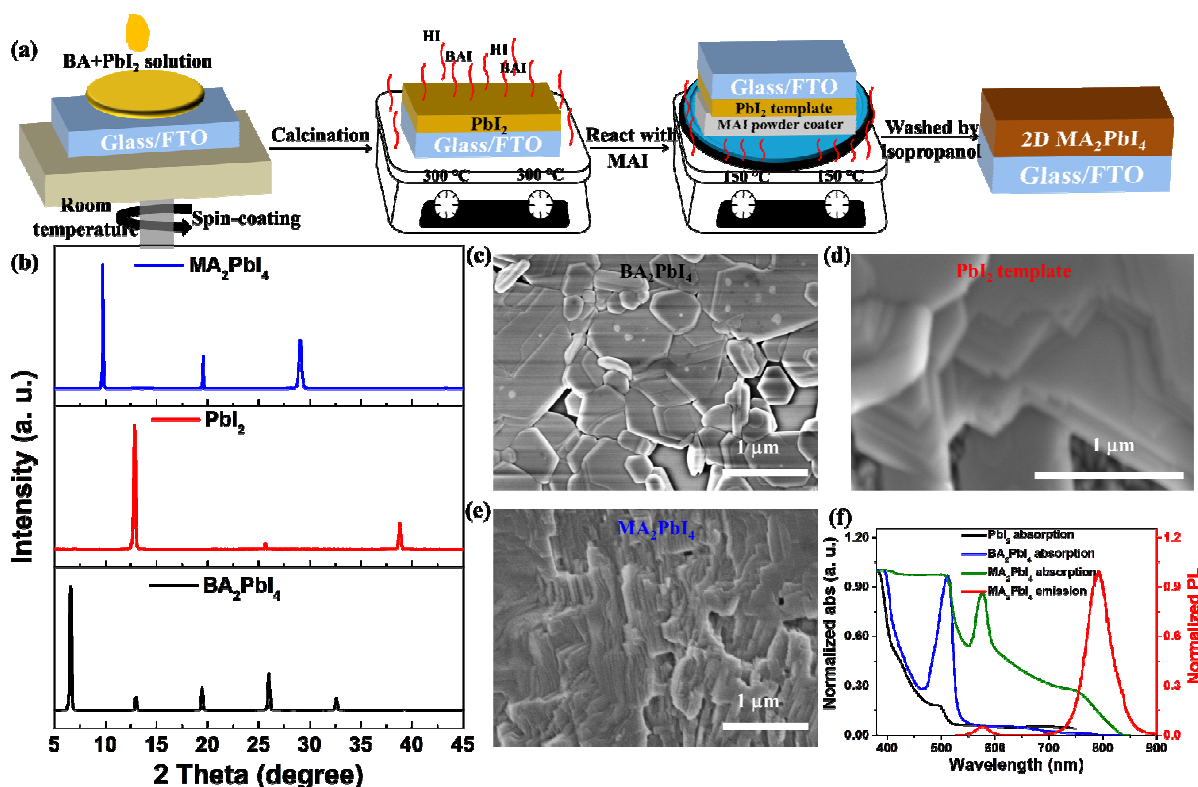


Fig. 1. (a) Schematic illustration of the fabrication process for MA₂PbI₄ perovskite film. (b) XRD spectra of BA₂PbI₄, PbI₂ template, and MA₂PbI₄. Corresponding top-view SEM images of (c) BA₂PbI₄, (d) PbI₂, and (e) MA₂PbI₄. (f) Absorbance spectra of PbI₂ template film, BA₂PbI₄ and MA₂PbI₄ films, and the PL emission for MA₂PbI₄.

was only 0.3%.²⁸ Almost immediately, 2D CH₃NH₃⁺ (MA)-based perovskite has been synthesized using combined solution process and vapor-phase conversion method. In fact, it has been studied for its application in photodetectors owing to its high photoluminescence quantum yield and unique band structure.²⁹ More recently, thiocyanide was used to substitute iodide to prepare 2D MA-based perovskite. It is found that with the pseudo-halogen substitution, the solar cell efficiency is increased to 3.32% with good stability.^{30,31} Even though there have been significant improvement in efficiency of the 2D PSCs, it is still lower compared to its 3D counterpart. Therefore, quasi-2D perovskite compounds, (C₆H₅C₂H₄NH₃)₂(MA)_{n-1}PbI_{3n+1}, where the bulky alkyl chain ammonium and short alkyl chain methylammonium cations are employed simultaneously, have been developed to reduce the exciton binding energy by increasing the proportion of the inorganic components (n), and the PCE of the 2D PSC was enhanced remarkably to 4.73%.³² Soon afterwards, Cao et al. adopted the shorter chain CH₃(CH₂)₃NH₃⁺ (BA) cations instead of C₆H₅C₂H₄NH₃⁺, yielding a PCE of 4.02% with a higher short-circuit current density (*J*_{sc}).¹⁵ The charge transport in 2D perovskite is expected to be highly confined within the QW plane as the electrons are freely movable in in-plane direction but tightly confined in out-of-plane direction. However, the charge transport in 2D perovskite devices is usually in out-of-plane direction, leading to unsatisfactory PCEs.¹² Later, a hot-coating deposition method was established to solve this problem by inducing preferential out-of-plane alignment of the inorganic perovskite component, which is beneficial to charge transport, and the PCE of 2D planar PSCs significantly increased to 12.52%.¹⁶ Moreover, there is a fatal disadvantage in that it is very difficult to precisely control the substrate temperature during the hot-coating procedure, resulting in inferior device reproducibility.

Therefore, an alternative 2D perovskite material with a reliable fabrication method is urgently needed to decrease both the exciton binding energy and the QW effect and to increase the conductivity.

Herein, we have developed a new strategy to fabricate highly crystalline 2D perovskite thin films with the preferred orientation using vapor-fumigation technology, where the shorter chains of MA⁺ were introduced as the organic spacing layers between the inorganic layers. The results from x-ray diffraction (XRD), scanning electron microscopy (SEM), and grazing incidence wide-angle x-ray scattering (GIWAXS) tests, as well as theoretical calculations demonstrate the successful formation of high-quality 2D MA-based perovskite films. Because of the material's excellent advantages, including the small exciton binding energy, reduced QW effect, higher conductivity, narrow band gap, low trap density, and strong resistance to moisture, the champion device based on the newly developed 2D perovskites yielded a PCE up to 16.92% (certified PCE of 16.6%) with reduced hysteresis, which is the highest value among the 2D devices reported. More importantly, the devices show good stability whether preserved in the dark or under continuous illumination. The unencapsulated 2D MA-based PSCs retained over 97.8% of their initial efficiencies after storage at ambient conditions with ~55% relative humidity for 1512 hours. After 500 hours of continuous illumination at 60 °C in Argon, the device's efficiency was 97.2% of its initial value. Even after following the illumination with light-soaking for over 500 h in ambient air, the PCE suffered only minor degradation of 3.8%. Thus, the new strategy provides a feasible method for fabricating high-efficiency, highly-stable 2D PSCs.

The corresponding XRD pattern shown in Fig. 1b reveals that the BA₂PbI₄ exclusively displays the overtones for (001), indicating that it preferentially grows along the (110) direction,^{33,34} which leads

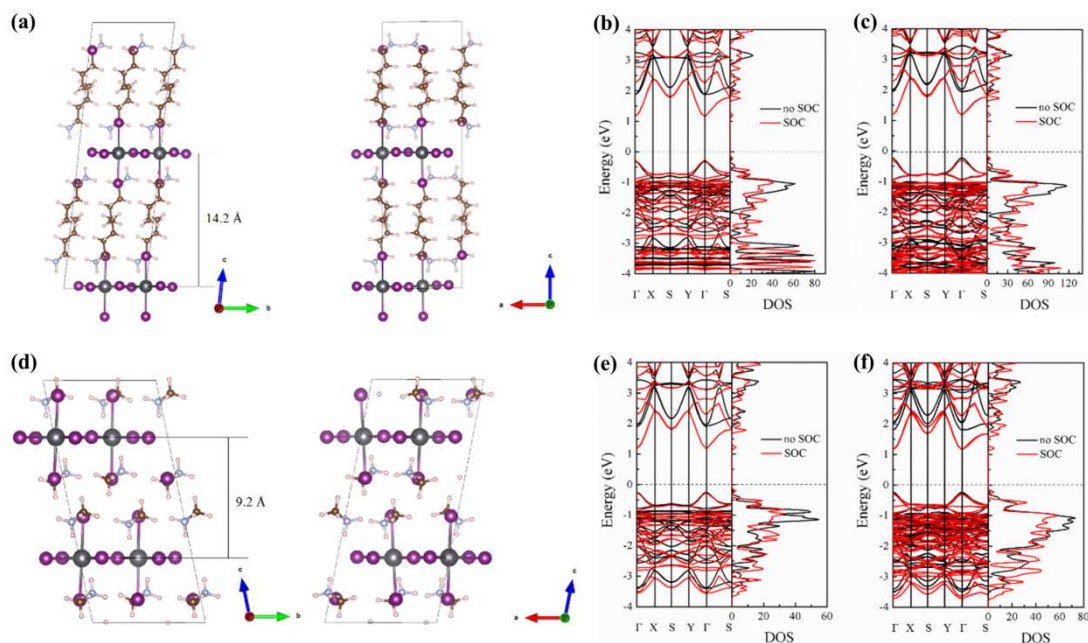


Fig. 2. (a) The structure configurations of (a) BA_2PbI_4 and (d) MA_2PbI_4 . DOS analysis of monolayer (b) BA_2PbI_4 and (e) MA_2PbI_4 , and bulk (c) BA_2PbI_4 and (f) MA_2PbI_4 with and without considering the SOC effect.

to the BA_2PbI_4 being orientated parallel to the substrate. Fig. 1c shows the top-view SEM image of the BA_2PbI_4 film. It is clear that the BA_2PbI_4 film is composed of nanosheets, and almost all the nanosheets are parallel to the substrate, in agreement with the XRD results. When the BA_2PbI_4 film was annealed at 300°C , the BA cations were removed (the high temperature led to BA_2PbI_4 decomposition, seen in Fig. S2), and the layered PbI_2 film formed (Fig. 1d). TXRD results in Fig. 1b show that the PbI_2 maintains the same orientation as the BA_2PbI_4 . The (001), (002) and (003) diffraction peaks are located at 12.86° , 25.66° and 38.80° , respectively.²⁹ It is clear that the (002) peak shifts toward larger angle compared to the BA_2PbI_4 (6.60°), apparently caused by the sharply reduced layer spacing from 13.39 \AA to 6.88 \AA , which can be calculated by the Bragg's law ($d = 2 \sin\theta/n\lambda$, where d is a layer spacing, n is an integer, λ is the X-ray wavelength, and θ is a half of diffraction angle).

It is found that the PbI_2 served as a template (Fig. 1d) when it was placed in contact with the MAI powder at 150°C . The MAI molecule entered between bilayers of the corner-sharing $[\text{PbI}_6]^{4-}$ octahedral to form the MA-based perovskite¹⁵. Fig. 1b shows the XRD pattern of the MA-based perovskite with the dominant peaks of (200) (400) and (101) located at 9.76° , 19.57° and 29.07° , respectively, all in excellent agreement with previously reported MA_2PbI_4 .³⁰ The layer spacing is significantly decreased to 9.08 \AA compared to BA_2PbI_4 (13.39 \AA) because shorter chain MA cations are introduced between the inorganic bilayers. The successful growth of the 2D MA_2PbI_4 crystalline film is also confirmed by the SEM analysis. Fig. 1e shows that the MA_2PbI_4 is composed of nanoslices, and these nanoslices are almost vertical with respect to the substrate, so the carriers can be transported along the nanoslices to arrive at the electrodes. Meanwhile, we fabricated the PbI_2 film using traditional spin-coating method, and then converted it into perovskite using vapor-fumigation of MAI. It is clear that the as prepared PbI_2 film is composed of scattered nanorods (Fig. S3a). When it is exposed to the MAI vapor, it is converted into perovskite (Fig. 3c). The XRD results (Fig. S3e) confirms the formation of traditional 3D perovskites.

We also performed GIWAXS by synchrotron radiation to gain insight into the orientation of the BA_2PbI_4 and MA_2PbI_4 perovskites, because GIXRD is an appropriate technique to study the crystal structure in different direction. Fig. S4a shows GIWAXS image of the BA_2PbI_4 film fabricated at room temperature. It is clear that its diffraction pattern is isotropic with the sample scatters equally in different directions, indicating that the crystal structure is not only in in-plane (q_{xy}) but also in out-of-plane (q_z), in agreement with previous report.¹⁶ However, MA_2PbI_4 perovskite fabricated by the present vapor-fumigation method exhibits sharp and discrete Bragg spots without noticeable arcs. Furthermore, the scattering pattern displays higher scattering intensity along q_z (Fig. S4b), demonstrating that the crystal structure is stacked in out-of-plane, in consistent with SEM result (Fig. 1e).

Fig. 1f shows the absorbance spectra of PbI_2 template film and different perovskite films deposited on quartz glass. It is apparent that the absorption peaks located at 496 nm , 512 nm and 575 nm belong to PbI_2 template film, BA_2PbI_4 and MA_2PbI_4 , respectively. The optical band gaps of different perovskite films are given in Fig. S5. It is clear that the BA_2PbI_4 has a wide band gap of 2.35 eV , and its absorption edge reaches only 528 nm , whereas the band gap of MA_2PbI_4 is 1.56 eV , and its absorption edge extends to 795 nm . Interestingly, the peak (located at 575 nm) above the absorption edge region appears in the MA_2PbI_4 . The peak above the absorption edge region is attributed to the quantum confinement and a long-lived trapped-exciton state generated by the MA ions around the negatively charged $[\text{PbI}_6]^{2-}$ layers.³¹ Another peak (751 nm) in MA_2PbI_4 close to the absorption edge region is originated from the multilayer stacked 2D perovskites.²⁹ The PL emission shows a weak emission in the high energy absorption peak (578 nm), in good accordance with the absorption. Efficient external luminescence is a highly desirable property for solar cells, because it is an indirect indication of efficient carrier generation, which enables a high open-circuit voltage (V_{oc}).³⁵

The structural parameters and electronic structures of BA_2PbI_4 and MA_2PbI_4 are calculated here to confirm our experimental results. The optimized lattice parameters of BA_2PbI_4 and MA_2PbI_4 including

the space group, lattice lengths and angle, and the layer spacing are calculated and displayed in Table S1, and the structure configurations are displayed in Fig. 2a and 2d. As can be seen, BA_2PbI_4 and MA_2PbI_4 all have triclinic structures, and the layer spacings of BA_2PbI_4 and MA_2PbI_4 are 14.2 and 9.2 Å, respectively, consistent with our experimental results, which further confirms the 2D structure of the MA_2PbI_4 samples.

In order to study the interlayer coupling between layers in BA_2PbI_4 and MA_2PbI_4 , the band structures and density of states (DOSs) of monolayer and bulk BA_2PbI_4 (Fig. 2b-c) and MA_2PbI_4 (Fig. 2e-f) with and without considering the spin-orbit coupling (SOC) effect are calculated. Direct band gaps of 2.16 and 2.04 eV are obtained for bulk BA_2PbI_4 (Fig. 2c) and MA_2PbI_4 (Fig. 2f), respectively, while band gaps of 2.19 and 2.06 eV are obtained for monolayer BA_2PbI_4 and MA_2PbI_4 , respectively, which indicates a weak interlayer coupling effect between layers in BA_2PbI_4 and MA_2PbI_4 . Once SOC effects were included in the band calculations, the band gaps of bulk BA_2PbI_4 and MA_2PbI_4 were considerably reduced to 1.44 and 1.41 eV due to band splitting, and similarly to 1.43 and 1.40 eV for monolayer BA_2PbI_4 and MA_2PbI_4 . The measured band gaps of BA_2PbI_4 are consistent with our calculated results without the SOC effect, while the band gaps of MA_2PbI_4 tend to match the values with the SOC effect, which indicates a stronger SOC effect in MA_2PbI_4 , likely due to the smaller layer spacing.

We also calculated the exciton binding energy of BA_2PbI_4 and MA_2PbI_4 . For the bulk 2D perovskite, the inorganic layer is considered as the well layer, and the organic layer is regarded as the barrier layer. According to the first-order perturbation theory and an infinite barrier approximation,³⁶ the exciton binding energy is determined by Eq (1),

$$E_b = 2 \frac{\epsilon_w - \epsilon_b}{\epsilon_w + \epsilon_b} \frac{e^2}{\epsilon_w d_w} \left(1 - e^{-\frac{1.7d_w}{a_0^*}}\right) \quad (1)$$

where d_w is the inorganic well thickness, a_0^* is the exciton effective Bohr radius, and ϵ_w and ϵ_b are the dielectric constants of the inorganic well layer and organic barrier layer, respectively. Thus, the exciton binding energy decreases with increasing dielectric constant as well as with narrower well-width. The inorganic well layer exhibits the dielectric constant of ca. 6,³⁷ and the dielectric constants of MA and BA are ~11 and ~4, respectively.^{38,39} For BA_2PbI_4 perovskite, the exciton binding energy is calculated to be ~510 meV, while the exciton binding energy of MA_2PbI_4 perovskite decreases to ~172 meV, consistent with the experimental results extracted from the absorption spectra (Fig. S6). Such a drastically reduced exciton binding energy leads to more free carriers in the MA_2PbI_4 film since there is less geminate recombination compared to BA_2PbI_4 film, leading to higher photocurrent in PSCs based on MA_2PbI_4 .

Particularly, the large energy barrier of the organic layer precludes carrier transport in out-of-plane direction.⁴⁰ Alternatively, out-of-plane charge transfer can occur through tunneling, which is restricted by the QW if the barrier height and barrier layer thickness are large. The tunneling probability through a QW structure can be calculated utilizing the WKB approximation and can be written as Eq (2).⁴¹

$$P_t(E) \approx e^{-\pi d_b \sqrt{\frac{2m\Delta E}{\hbar^2}}} \quad (2)$$

where d_b is the organic barrier thickness, ΔE is the barrier height, \hbar is Planck's constant, and m is the free electron mass. We assumed that a reasonable bandgap of the barrier layer is approximately 6 eV,⁴² and the probability of the free carriers tunneling through a single organic barrier in BA_2PbI_4 is calculated to be 2.3×10^{-7} , indicating negligible out-of-plane carrier transfer through multiple barrier layers. From the XRD spectra, we can see that the layer

spacings of BA_2PbI_4 and MA_2PbI_4 are 13.39 and 9.08 Å (Fig. 1b), respectively; thus the MA barrier thickness is reduced by 4.31 Å. The tunneling probability in the MA_2PbI_4 is thereby increased to 8.2×10^{-3} , which means that carrier transfer in out-of-plane direction becomes possible, corresponding to its good conductivity.

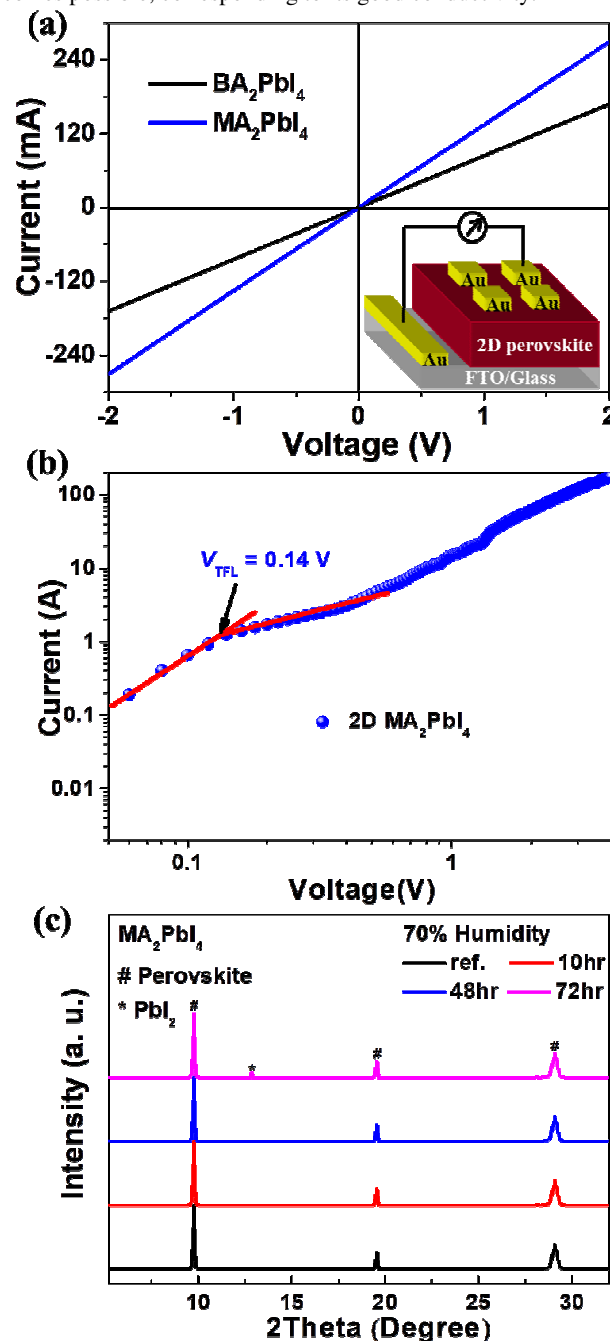


Fig. 3. (a) I - V characteristics of BA_2PbI_4 and MA_2PbI_4 films deposited on FTO substrates. The inset shows the relevant device structure. (b) Dark I - V curves of the MA_2PbI_4 devices revealing V_{TFL} kink point behavior. (c) XRD spectra of MA_2PbI_4 stored at 70% humidity for different time intervals.

The conductivity and trap density play important roles in PSCs.^{43,44} We therefore deposited BA_2PbI_4 and MA_2PbI_4 films on FTO substrates to probe their conductivities. Fig. 3a presents the current-voltage (I - V) curves with the device structure schematically illustrated in the inset and the key characteristics listed in Table S2.

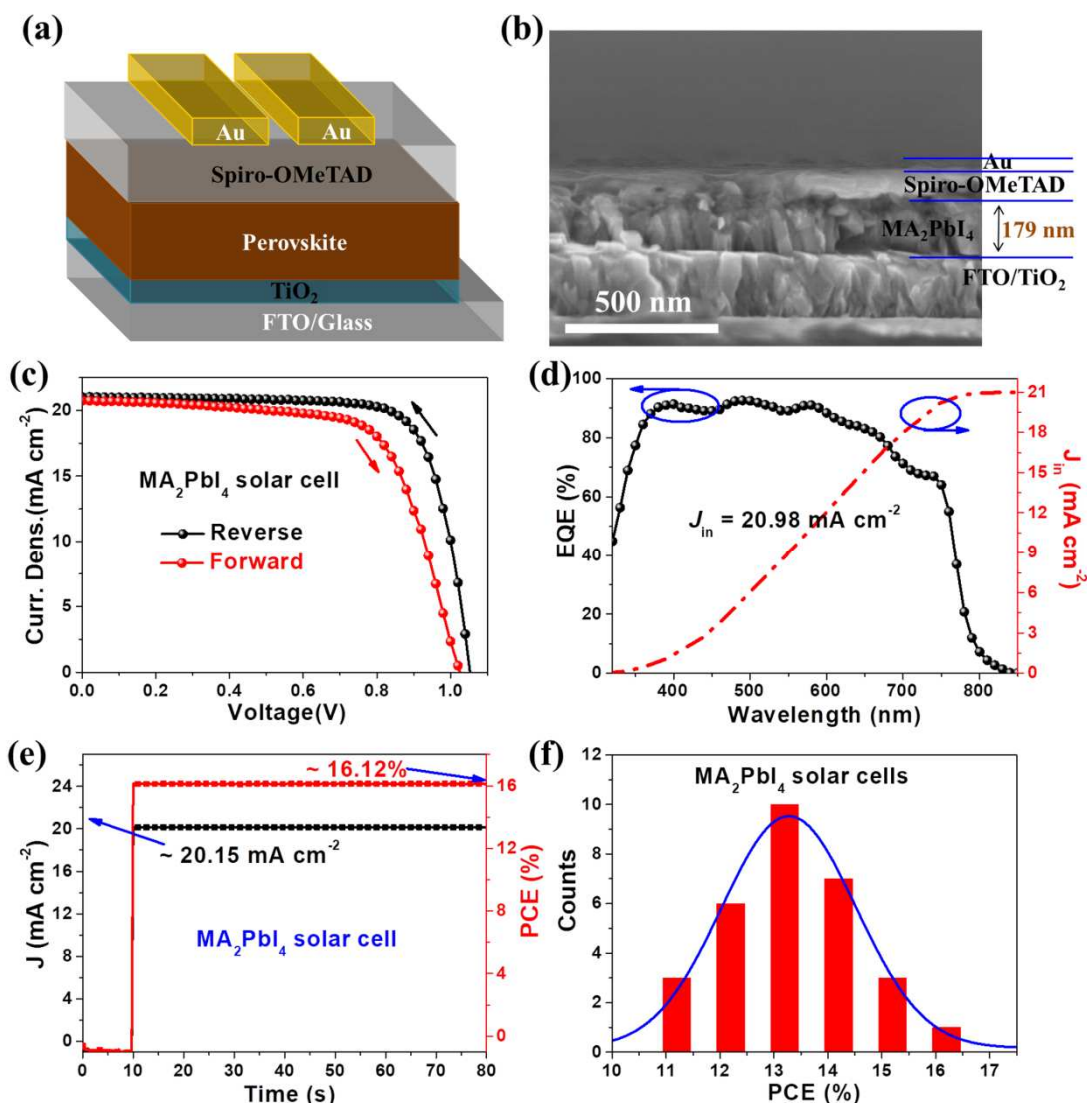


Fig. 4. (a) Illustration of the structure of the PSCs. (b) Cross-sectional SEM of a completed device based on a MA_2PbI_4 absorber. (c) The J - V curves of a MA_2PbI_4 solar cell under both reverse and forward scan directions. (d) Corresponding EQE and integrated J_{sc} of the champion device. (e) Photocurrent density and PCE measured as a function of time biased at 0.80 V for the champion MA_2PbI_4 solar cell. (f) Histogram of the PCE distribution for 30 devices based on MA_2PbI_4 .

Table 1. The key J - V parameters and hysteresis indices of MA_2PbI_4 and BA_2PbI_4 solar cells measured under AM 1.5G illumination at 100 mW cm^{-2} .

Solar cell	Scan direction	J_{sc} (mA cm^{-2})	V_{oc} (V)	FF	PCE (%)	HI
MA_2PbI_4	reverse	21.00	1.06	0.76	16.92	0.07
	forward	20.73	1.02	0.68	14.38	
BA_2PbI_4	reverse	1.14	0.90	0.39	0.40	0.28
	forward	1.01	0.89	0.30	0.27	

Compared to the BA_2PbI_4 film, the electrical conductivity of the MA_2PbI_4 increases to 2.96×10^{-3} from $1.53 \times 10^{-3} \text{ mS cm}^{-1}$. The high conductivity is likely attributed to the small layer spacing and large tunneling probability.

Fig. 3b shows the dark I - V of MA_2PbI_4 films in devices with a FTO/perovskite/Au structure. The linear relation indicates an ohmic

contact at low bias voltages in these devices. When the bias voltage exceeds the kink point, the current quickly increases nonlinearly because the trap states are completely filled. The trap density is determined from the trap-filled limit voltage (V_{TFL}) according to Eq (3):⁴⁵

$$n_t = \frac{2\epsilon_0\epsilon V_{\text{TFL}}}{eL^2} \quad (3)$$

where e is the elementary charge of the electron, L is the thickness of the film, ϵ is the relative dielectric constant of perovskite,⁴⁶ and ϵ_0 is the vacuum permittivity. The calculated trap density for MA_2PbI_4 film is $4.36 \times 10^{15} \text{ cm}^{-3}$, lower than the value for the 3D perovskite of $\sim 10^{16} \text{ cm}^{-3}$ (Fig. S7). The low trap density is attributed to the excellent film quality, which is beneficial to improving the device performance.⁴⁷

The stability of bare MA_2PbI_4 in humidity was monitored by XRD, as shown in Fig. 3c. We exposed the sample films to 70%

humidity without any protection for different time intervals. The MA₂PbI₄ film displayed good crystallinity without any other impurity peaks after 48 h. However, the 3D MAPbI₃ perovskite exhibited the PbI₂ phase due to degradation by moisture after 10 h (Fig. S8). After exposure for 72 h, the tiny signature peaks of PbI₂ were detected in both MA₂PbI₄ films. The significantly improved stability in the moist environment is ascribed to the well-ordered crystallization in the MA₂PbI₄ perovskite films. In brief, the superior resistance of the MA₂PbI₄ to humidity makes it a promising candidate for the active material of perovskite solar cells for potential commercial applications.

Given its unique advantages, we introduced the 2D MA₂PbI₄ perovskite film into devices to further investigate its photoelectric properties. The device architecture and cross-sectional SEM of the complete device are shown in Fig. 4a and 4b. Additionally, PSCs based on BA₂PbI₄ absorbers were fabricated for comparison. Fig. 4c gives the current density-voltage (*J-V*) curves of the champion MA₂PbI₄ device tested in both reverse and forward scan directions under AM 1.5G (air mass 1.5 global 1-Sun) illumination with a scan rate of 0.1 V s⁻¹. Table 1 summarizes the key parameters including *J*_{sc}, *V*_{oc}, fill factor (FF), PCE and hysteresis index (HI). The PCE of the device employing MA₂PbI₄ is as high as 16.92% with *J*_{sc} of 21.00 mA cm⁻², *V*_{oc} of 1.06 V, and FF of 0.76. To the best of our knowledge, this is the highest PCE reported to date for 2D PSCs. The certified PCE is 16.6%, and the certificate is shown in Fig. S9. Compared to 3D PSCs, the relatively low *V*_{oc} of the MA₂PbI₄ solar cell is mainly caused by the large exciton binding energy of 2D perovskites, leading to increased energy loss in the device.⁴⁸ The PCE of the BA₂PbI₄ device is only 0.40% (Fig. S10) owing to inferior orientation for carrier transport.^{12,13,49} Surprisingly, the efficiency of the MA₂PbI₄ device enormously increased by over 40 times compared to that of the BA₂PbI₄ cell. The small exciton binding energy, high carrier tunneling probability between the planes, good conductivity and low trap density of MA₂PbI₄ lead to high performance of the solar cells.

Meanwhile, we also studied the hysteresis effect in PSCs, and the hysteresis index was defined as Eq (4):⁵⁰

$$HI = \frac{J_{RS}(0.5V_{oc}) - J_{FS}(0.5V_{oc})}{J_{RS}(0.5V_{oc})} \quad (4)$$

where *J*_{RS} (0.5 *V*_{oc}) and *J*_{FS} (0.5 *V*_{oc}) are the current densities at a voltage equal to half of *V*_{oc} in the reverse and forward scans, respectively. The MA₂PbI₄ device has the smallest hysteresis index (0.07) compared to the BA₂PbI₄ devices (0.28). Generally, the hysteresis in PSCs is caused by ion migration, trap density, imbalance charge transport between hole transport layer and electron transport layer.^{51,52} The reduced hysteresis in MA₂PbI₄ solar cells originates from suppressed ion migration and inhibited carrier recombination due to the good orientation and low trap density.^{53,54} Furthermore, the smaller hysteresis presented in the MA₂PbI₄ devices is likely caused by imbalanced charge transport between 2,2',7,7'-tetrakis(N,N-di-p-methoxyphenylamine)-9,9'-spirobifluorene (spiro-OMeTAD) (the hole mobility is about 10⁻³ cm² V⁻¹ s⁻¹) and TiO₂ (the electron mobility is about 10⁻⁴ cm² V⁻¹ s⁻¹).⁴⁷

Fig. 4d shows the external quantum efficiency (EQE) and the integrated *J*_{sc} of the MA₂PbI₄ device. The EQE spectrum cuts off at ca. 800 nm, in good agreement with its absorbance spectrum (Fig. S11), and the fast decline beyond 650 nm results from the weak absorption of the thin MA₂PbI₄ absorber layer (179 nm, see Fig. 4b). The integrated *J*_{sc} from the EQE curves with the AM 1.5G photon flux is up to 20.98 mA cm⁻², in excellent agreement with the direct *J-V* measurements. The photocurrent density vs. time and PCE vs. time curves of the MA₂PbI₄ device were measured at *V*_{mp} (voltage at the maximum power point) to confirm the realized PCE, as shown in

Fig. 4e. The photocurrent density and PCE rapidly stabilize at 20.15 mA cm⁻² and 16.12%, respectively, demonstrating that the *J-V* measurement is reliable. We further investigated the reproducibility of MA₂PbI₄ solar cells, and 30 devices were fabricated to gather performance statistics. Fig. 4f displays the PCE distribution histogram, and their key parameters are listed in Table S3. The average PCE reaches 14.18 ± 1.40% with average *J*_{sc} = 20.88 ± 1.36 mA cm⁻², *V*_{oc} = 0.98 ± 0.04 V and FF = 0.73 ± 0.06. It seems that the average values have fairly small error distributions, implying that MA₂PbI₄ PSCs exhibit good reproducibility. The new vapor-fumigation method not only significantly enhanced the efficiency but also efficiently solves the reproducibility problems faced by other methods.

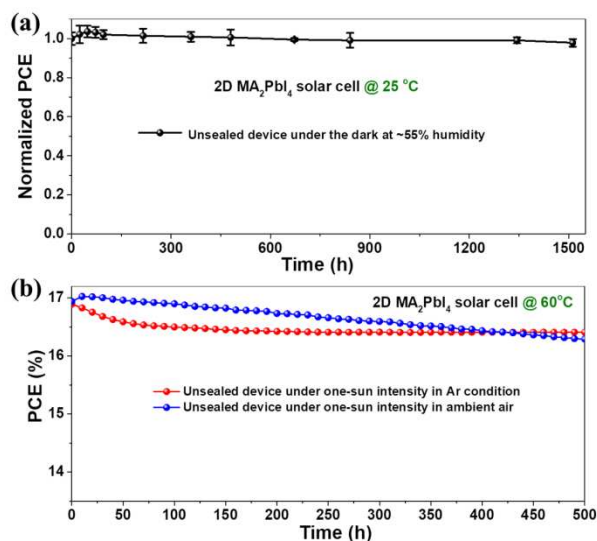


Fig. 5. (a) Long-term stability of MA₂PbI₄ solar cells without any encapsulation stored at ~55% RH in the dark. (b) Continuous illumination stability of a MA₂PbI₄ device in different atmospheres at 60 °C.

Furthermore, we studied the long-term stability of PSCs based on MA₂PbI₄. The bare devices without any encapsulation were stored in the lab ambient environment with relative humidity of ~55%. Eight representative devices were selected from different batches of the respective MA₂PbI₄ devices, with *J-V* measurements taken at various time intervals. Fig. 5a gives a representative set of normalized PCEs as a function of test time. Surprisingly, the MA₂PbI₄ devices maintained 97.8% of their initial efficiency after 1512 h. The continuous illumination stability was also investigated. Fig. 5b shows the PCE of a MA₂PbI₄ device under continuous illumination measured in different atmospheres. The device maintains 97.2% of its initial efficiency under continuous illumination after 500 h at 60 °C in Ar. Even after following the illumination with light-soaking for over 500 h in ambient air, the unsealed device suffered only minor degradation of 3.8%. Compared to the device stored in Ar, an increased performance of solar cell stored in ambient air at the primary stage is contributed to the oxidation of spiro-OMeTAD. It is known that the spiro-OMeTAD often needs some oxidation (by oxygen or air) to attain increased conductivity.⁵⁵ When the measurement is extended to over 400 hours, performance of the perovskite solar cell degrades more in air than that in Ar. The prolonged environmental stability of MA₂PbI₄ devices is consistent with the large van der Waals interaction, as confirmed in previous reports.^{16,29}

Conclusions

In conclusion, 2D MA₂PbI₄ perovskite has been successfully fabricated using a vapor-fumigation method. The PCE of the PSCs utilizing the MA₂PbI₄ perovskite is as high as 16.92% (certified PCE at 16.6%), the highest efficiency reported to date for 2D PSCs. More importantly, the 2D MA₂PbI₄ PSCs display surprisingly better long-term stability regardless of whether they were stored in the dark or under illumination. Theoretical and experimental results reveal that the excellent performance is ascribed to the outstanding optoelectronic properties of the 2D MA₂PbI₄, such as a small exciton binding energy, high carrier tunneling probability in out-of-plane direction, narrow band gap, good conductivity, and strong resistance to environmental stimuli. The high efficiency and superior stability demonstrate that the present method provides a promising pathway towards high quality 2D perovskites for potential commercial applications.

Author contribution

D. Yang and X. Zhu designed and performed all experiments. Z. Xu helped with calculated results. S. Zuo and J. Feng helped with TGA and SEM results. Z. Wang tested the PL spectra. K. Zhao helped with GIWAXS measurements. X. Zhang, J. Zhang and H. Liu contributed helpful suggestions for this paper. D. Yang wrote the first draft of the paper. D. Yang, S. (Frank) Liu and S. Priya supervised the overall project, discussed the results, and contributed to the final manuscript.

Acknowledgements

The authors acknowledge support from the National Key Research Development Program of China (2016YFA0202403), the National Natural Science Foundation of China (61604090/91733301). D. Yang acknowledges the financial support from NSFI/UCRC: Center for Energy Harvesting Materials and Systems (CEHMS). S. Priya acknowledges the financial support from Air Force office of Scientific Research under award number: FA9550-17-1-0341. S. Liu would like to acknowledge the support from the National University Research Fund (GK261001009), the Innovative Research Team (IRT_14R33), the 111 Project (B14041) and the Chinese National 1000-Talent-Plan program. J. Zhang acknowledges financial support from the Bagui Scholars Program of Guangxi.

Notes and references

^aKey Laboratory of Applied Surface and Colloid Chemistry, National Ministry of Education; Shaanxi Engineering Lab for Advanced Energy Technology, School of Materials Science and Engineering, Shaanxi Normal University, Xi'an 710119, China

^bState Key Laboratory of Catalysis, Dalian National Laboratory for Clean Energy, Dalian Institute of Chemical Physics, Chinese Academy of Sciences, Dalian, 116023, China

^cMaterials Science and Engineering, Penn State, University Park, PA 16802, United States

^dGuangxi Key Laboratory of Information Materials, School of Materials Science and Engineering, Guilin University of Electronic Technology, Guilin, 541004, China

*E-mail: spriya@vt.edu; szliu@dicp.ac.cn; dongyang@snnu.edu.cn

Electronic Supplementary Information (ESI) available: [details of any supplementary information available should be included here]. See DOI:10.1039/c000000x/

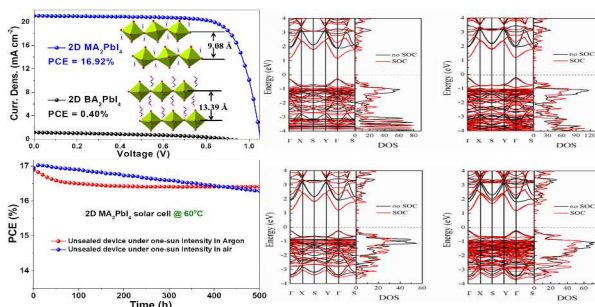
1 G. E. Eperon, T. Leijtens, K. A. Bush, R. Prasanna, T. Green, J. T.-W.

- Wang, D. P. McMeekin, G. Volonakis, R. L. Milot, R. May, A. Palmstrom, D. J. Slotcavage, R. A. Belisle, J. B. Patel, E. S. Parrott, R. J. Sutton, W. Ma, F. Moghadam, B. Conings, A. Babayigit, H.-G. Boyen, S. Bent, F. Giustino, L. M. Herz, M. B. Johnston, M. D. McGehee and H. J. Snaith, *Science* 2016, **354**, 861-865.
- 2 D. Yang, R. Yang, X. Ren, X. Zhu, Z. Yang, C. Li and S. Liu, *Adv. Mater.* 2016, **28**, 5206-5213.
- 3 Q.-Q. Ge, J.-Y. Shao, J. Ding, L.-Y. Deng, W.-K. Zhou, Y.-X. Chen, J.-Y. Ma, L.-J. Wan, J. Yao, J.-S. Hu and Y.-W. Zhong, *Angew. Chem. Int. Ed.* DOI:10.1002/anie.201806392.
- 4 Q. Dong, Y. Fang, Y. P. Shao, J. Mulligan, Qiu, L. Cao and J. Huang, *Science* 2015, **347**, 967-970.
- 5 M. Saliba, J.-P. Correa-Baena, M. Grätzel, A. Hagfeldt and A. Abate, *Angew. Chem. Int. Ed.* 2018, **57**, 2554-2569.
- 6 Z. Xiao, Q. Dong, C. Bi, Y. Shao, Y. Yuan and J. Huang, *Adv. Mater.* 2014, **26**, 6503-6509.
- 7 E. Castro, T. J. Sisto, E. L. Romero, F. Liu, S. R. Peurifoy, J. Wang, X. Zhu, C. Nuckolls and L. Echegoyen, *Angew. Chem. Int. Ed.* 2017, **56**, 14648-14652.
- 8 J. Burschka, N. Pellet, S.-J. Moon, R. Humphry-Baker, P. Gao, M. K. Nazeeruddin and M. Grätzel, *Nature* 2013, **499**, 316-319.
- 9 M. Liu, M. B. Johnston and H. J. Snaith, *Nature* 2013, **501**, 395-398.
- 10 W. S. Yang, B.-W. Park, E. H. Jung, N. J. Jeon, Y. C. Kim, D. U. Lee, S. S. Shin, J. Seo, E. K. Kim, J. H. Noh and S. Seok, *Science* 2017, **356**, 1376-1379.
- 11 A. Kojima, K. Teshima, Y. Shirai and T. Miyasaka, *J. Am. Chem. Soc.* 2009, **131**, 6050-6051.
- 12 Y. Chen, Y. Sun, J. Peng, J. Tang, K. Zheng and Z. Liang, *Adv. Mater.* 2018, **30**, 1703487.
- 13 X. Zhang, X. Ren, B. Liu, R. Munir, X. Zhu, D. Yang, J. Li, Y. Liu, D.-M. Smilgies, R. Li, Z. Yang, T. Niu, X. Wang, A. Amassian, K. Zhao and S. Liu, *Energy Environ. Sci.* 2017, **10**, 2095-2102.
- 14 J. Liu, J. Leng, K. Wu, J. Zhang and J. Shengye, *J. Am. Chem. Soc.* 2017, **139**, 1432-1435.
- 15 D. H. Cao, C. C. Stoumpos, O. K. Farha, J. T. Hupp and M. G. Kanatzidis, *J. Am. Chem. Soc.* 2015, **137**, 7843-7850.
- 16 H. Tsai, W. Nie, J.-C. Blancon, C. C. Stoumpos, R. Asadpour, B. Harutyunyan, A. J. Neukirch, R. Verduzco, J. J. Crochet, S. Tretiak, L. Pedesseau, J. Even, M. A. Alam, G. Gupta, J. Lou, P. M. Ajayan, M. J. Bedzyk, M. G. Kanatzidis and A. D. Mohite, *Nature* 2016, **536**, 312-316.
- 17 J. Qing, X.-K. Liu, M. Li, F. Liu, Z. Yuan, E. Tiukalova, Z. Yan, M. Duchamp, S. Chen, Y. Wang, S. Bai, J.-M. Liu, H. J. Snaith, C.-S. Lee, T. C. Sum and F. Gao, *Adv. Energy Mater.* 2018, **8**, 1800185.
- 18 L. N. Quan, M. Yuan, R. Comin, O. Voznyy, E. M. Beauregard, S. Hoogland, A. Buin, A. R. Kirmani, K. Zhao, A. Amassian, D. H. Kim and E. H. Sargent, *J. Am. Chem. Soc.* 2016, **138**, 2649-2655.
- 19 K. Kikuchi, Y. Takeoka, M. Rikukawa and K. Sanui, *Curr. Appl. Phys.* 2004, **4**, 599-602.
- 20 H. Y. Schlipf, J. Schlipf, M. Wussler, M. L. Petrus, W. Jaegermann, T. Bein, P. Müller-Buschbaum and P. Docampo, *ACS Nano* 2016, **10**, 5999-6007.
- 21 C. Huang, Y. Gao, S. Wang, C. Zhang, N. Yi, S. Xiao and Q. Song, *Nano Energy* 2017, **41**, 320-326.
- 22 C. Lerner, S. T. Birkhold, I. L. Moudrakovski, P. Mayer, L. M. Schoop, L. Schmidt-Mende and B. V. Lotsch, *Chem. Mater.* 2016, **28**, 6560-6566.
- 23 X. Hong, T. Ishihara and A. V. Nurmikko, *Phys. Rev. B* 1992, **45**, 6961-6964.
- 24 T. Ishihara, J. Takahashi and T. Goto, *Phys. Rev. B* 1990, **42**, 11099-11107.
- 25 M. Era, S. Morimoto, T. Tsutsui and S. Saito, *Appl. Phys. Lett.* 1994, **65**, 676-678.
- 26 M. Shimizu, J.-I. Fujisawa and T. Ishihara, *Phys. Rev. B* 2006, **74**, 155206.
- 27 K. Gauthron, J.-S. Lauret, L. Doyennette, G. Lanty, A. A. Choueiry, S. J. Zhang, A. Brehier, L. Largeau, O. Mauguin, J. Bloch and E. Deleporte, *Opt. Exp.* 2010, **18**, 5912-5919.
- 28 S. Ahmad, P. K. Kanaujia, H. J. Beeson, A. Abate, F. Deschler, D. Credgington, U. Steiner, G. V. Prakash and J. J. Baumberg, *ACS Appl. Mater. Interfaces* 2015, **7**, 25227-25236.
- 29 J. Liu, Y. Xue, Z. Wang, Z.-Q. Xu, C. Zheng, B. Weber, J. Song, Y. Wang, Y. Lu, Y. Zhang and Q. Bao, *ACS Nano* 2016, **10**, 3536-3542.

- 30 J. Liu, J. Shi, D. Li, F. Zhang, X. Li, Y. Xiao and S. Wang, *Synthetic Metals* 2016, **215**, 56-63.
- 31 Y. Lv, D. Si, X. Song, K. Wang, S. Wang, Z. Zhao, C. Hao, L. Wei and Y. Shi, *Inorg. Chem.* 2018, **57**, 2045-2050.
- 32 I. C. Smith, E. T. Hoke, D. Solis-Ibarra, D. M. McGehee and H. I. Karunadasa, *Angew. Chem., Int. Ed.* 2014, **53**, 11232-11235.
- 33 C. Huo, B. Cai, Z. Yuan, B. Ma and H. Zeng, *Small* 2017, **1**, 1600018.
- 34 D. B. Mitzi, *J. Mater. Chem.* 2004, **14**, 2355-2365.
- 35 O. D. Miller, E. Yablonovitch and S. R. Kurtz, *IEEE J. Photovoltaics* 2012, **2**, 303-311.
- 36 H. Mathieu, P. Lefebvre and P. Christol, *Phys. Rev. B* 1992, **46**, 4092-4101.
- 37 E. A. Muljarov, S. G. Tikhodeev, N. A. Gippius and T. Ishihara, *Phys. Rev. B* 1995, **51**, 14370-14378.
- 38 W. T. Cronenwett and L. W. Hoogendoorn, *J. Chem. Eng. Data* 1972, **17**, 298-300.
- 39 A. L. Powell and A. E. Martell, *J. Am. Chem. Soc.* 1957, **79**, 2118-2123.
- 40 A. Szafer and A. D. Stone, *Phys. Rev. Lett.* 1989, **62**, 300-303.
- 41 J. Gain, M. D. Sarkar and S. Kundu, *arXiv:1002.1931* 2010, 1-8.
- 42 K. Pradeesh, J. J. Baumberg and G. V. Prakash, *Opt. Express* 2009, **17**, 22171.
- 43 X. Ren, D. Yang, Z. Yang, J. Feng, X. Zhu, J. Niu, Y. Liu, W. Zhao and S. Liu, *ACS Appl. Mater. Interfaces* 2017, **9**, 2421-2429.
- 44 M. He, B. Li, X. Cui, B. Jiang, Y. He, Y. Chen, D. O'Neil, P. Szymanski, M. A. El-Sayed, J. Huang and Z. Lin, *Nat. Commun.* 2017, **8**, 16045.
- 45 R. H. Bube, *J. Appl. Phys.* 1962, **33**, 1733-1737 (1962).
- 46 A. Poglitsch and D. Weber, *J. Chem. Phys.* 1987, **87**, 6373-6378.
- 47 D. Yang, X. Zhou, R. Yang, Z. Yang, Y. Wei, X. Wang, C. Li, S. Liu and R. P. H. Chang, *Energy Environ. Sci.* 2016, **9**, 3071-3078.
- 48 G. Grancini, C. Roldán-Carmona, I. Zimmermann, E. Mosconi, X. Lee, D. Martineau, S. Narbey, F. Oswald, F. D. Angelis, M. Graetzel and M. K. Nazeeruddin, *Nat. Commun.* 2017, **8**, 15684.
- 49 M. I. Saidaminov, O. F. Mohammed and O. M. Bakr, *ACS Energy Lett.* 2017, **2**, 889-896.
- 50 M. Valles-Pelarda, B. C. Hames, I. García-Benito, O. Almora, A. Molina-Ontoria, R. S. Sánchez, G. Garcia-Belmonte, N. Martín and I. Mora-Sero, *J. Phys. Chem. Lett.* 2016, **7**, 4622-4628.
- 51 B. Chen, M. Yang, S. Priya and K. Zhu, *J. Phys. Chem. Lett.* 2016, **7**, 905-917.
- 52 N. Tessler and Y. Vaynzof, *ACS Appl. Energy Mater.* 2018, **1**, 676-683.
- 53 J. Chen, D. Lee and N.-G. Park, *ACS Appl. Mater. Interfaces* 2017, **9**, 36338-36349.
- 54 T. Zhang, M. I. Dar, G. Li, F. Xu, N. Guo, M. Grätzel and Y. Zhao, *Sci. Adv.* 2017, **3**, e1700841.
- 55 X. Zhu, D. Yang, R. Yang, B. Yang, Z. Yang, X. Ren, J. Zhang, J. Niu, J. Feng and S. Liu, *Nanoscale* 2017, **9**, 12316-12323.

Table of content

The record efficiency of two-dimensional perovskite solar cell reaches to 16.92% (certified at 16.6%) with excellent stability using vapor-fumigation technique.



Broader Context

Even though the efficiency of perovskite solar cell rapidly increases to 23.3% due to the outstanding properties of perovskites, their environmental instability becomes a major issue, which limits the commercialization application. Recently, Ruddlesden-Popper two-dimensional (2D) perovskite materials exhibit superior stability owing to their beneficial geometric effect and dielectric contrast effect, unfortunately, the efficiency of 2D perovskite solar cell is much lower because of severe charge recombination affected by large exciton binding energy, poor carrier transport caused by quantum wells, and low conductivity produced by insulating bulky organic spacer cations. In present work, we developed vapor-fumigation technique to fabricate methylammonium based 2D perovskite, the high dielectric constant and short-chain of methylammonium lead to smaller exciton binding energy, better conductivity and good carrier transport compared to traditional 2D perovskite based on bulky butylammonium. In addition, theoretical calculation and experimental analysis reveal that methylammonium based 2D perovskites possess strong tunneling probability of a carrier through a quantum well and ideal band gap. As a result, the efficiency of 2D methylammonium based perovskite solar cells is up to as high as 16.92%, and certified efficiency is 16.6%, the highest reported so far for 2D perovskite solar cells. Moreover, our 2D perovskite devices exhibited superior stability under illumination and exposure to environmental conditions. The efficiency of unsealed 2D perovskite device remains 97.8% of its initial value when exposed to ambient conditions at about 55% relative humidity for 1512 hours. Even after following the illumination test with light-soaking for over 500 h in ambient air, the PCE of the unsealed device suffered only a minor degradation of 3.8%. The high efficiency, vastly superior stability, and ease of fabrication demonstrate that the present technique provides a promising pathway toward fabricating 2D perovskite photovoltaics with high performance.